Characterization of parasitic gratings in $LiNbO_3$

M. Fally, M. A. Ellabban, R. A. Rupp, M. Fink, and J. Wolfsberger
Institut für Experimentalphysik, Universität Wien, Strudlhofgasse 4, A-1090 Wien, Austria

E. Tillmanns
Institut für Mineralogie und Kristallographie, Universität Wien, Althanstraße 14, A-1090 Wien, Austria
(Received 7 September 1999)

We present a detailed experimental study of photoinduced light scattering in $LiNbO_3$:Fe. The transmitted intensity was investigated as a function of the read-out wavelength and of the reconstruction angle for two different rotation axes. A simple phenomenological model based on the Ewald construction is developed which explains the characteristic features of the angular and spectral dependence of the transmitted intensity in the presence of parasitic gratings.

I. INTRODUCTION

Holographic recording processes are usually accompanied by a rise of unintentional photoinduced light scattering,[1] so-called holographic scattering. As the primary beam interferes with light scattered from inhomogeneities, small refractive index changes are generated via the photorefractive effect from which light is diffracted additionally, hence leading to an increase of the refractive index change if the diffracted wave adds constructively to the scattered wave. This process naturally is time dependent and as a rule strives for a stationary state, i.e., the intensity of the scattered light increases up to a maximum.[2] The photoinduced structure of refractive index inhomogeneities can be regarded as a host of parasitic gratings. Those spurious structures, which are recorded at the same time as the desired holograms, reduce the diffraction efficiency and lead to a reduction in the image quality during hologram reconstruction. As they limit data storage applications, it is an important task to study their genesis, as well as the functional dependence of the intensity of a reconstructing wave on various parameters such as wavelength, reconstruction angle (RA), and its polarization. On the other hand, holographic scattering provides also valuable insight into the dynamics of holographic recording processes.[1,3,4] Only recently, holographic scattering has attracted renewed attention when it was discovered even in centrosymmetric crystals in which light amplification on the basis of wave mixing is forbidden.[5]

In the present work we study the genesis and evolution of parasitic gratings by using a single beam setup, and investigate the angular and spectral dependence of the transmittance of a reconstructing light wave in the presence of the established refractive index inhomogeneity (i.e., the pattern in the stationary state). Furthermore, we apply a phenomenological model based on the Ewald construction,[6,7] describing qualitatively the measured dependences when reconstructing the autogenerated holograms. This is of some importance as it will give a hint on how to choose suitable reconstruction conditions at which their effect can be minimized.

II. EXPERIMENT

The experiments were carried out on an oxidized $LiNbO_3$:Fe crystal (742-05/Ox) with an iron content of 0.1 wt.% Fe_2O_3 in the melt and dimensions of $a\times b\times c = 17.9\times 2.55\times 9.6\ \mathrm{mm}^3$. Parasitic gratings in $LiNbO_3$:Fe were generated by a single extraordinarily polarized laser beam of diameter 4 mm hitting the crystal at normal incidence and propagating through it along a direction perpendicular to the c axis of the crystal. The recording time was typically 10 min at an intensity of $I_p = 0.2\ \mathrm{W\,cm^{-2}}$, i.e., with an exposure of about 100 J cm^{-2}, the wavelengths being either $\lambda_p = 514$ nm or $\lambda_p = 488$ nm. The transmitted intensity was detected by a silicon diode (diameter 5 mm) and the amplified signal collected by a computer. The faces perpendicular to the c axis were short circuited to avoid build-up of pyroelectric and photovoltaic fields across the sample. The sample was fixed on a holder placed on a high-precision rotation stage ($\pm 10^{-3}$deg) which allowed for a rotation around two axes that were mutually perpendicular.

One characteristic feature of holographic scattering is its time dependence. Following an approach[2] to describe the transmitted intensity as a function of the recording time yields [Eq. (6) in Ref. 2]

$$\frac{I_p(t)}{I_p(0)} = \frac{1+m_0}{1+m_0\exp(\Gamma_e d)}, \qquad \Gamma_e(t) = \Gamma[1-\exp(-t/\tau)]. \tag{1}$$

Here d is the thickness of the sample, while Γ, τ, and m_0 are fit parameters which may be interpreted as gain, dielectric relaxation time, and the fraction of the initially (i.e., at $t=0$) scattered intensity, respectively. In Fig. 1 the transmitted intensity during the writing process is shown for $\lambda_p = 488$ nm. The solid line gives the fit to Eq. (1) and describes the recording behavior excellently ($\chi^2 = 2\times 10^{-5}$) despite the simplicity of the applied model. The fit parameters are $\Gamma = (2.32\pm 0.01)\ \mathrm{mm}^{-1}$, $\tau = (118\pm 0.5)$ sec, and $m_0 = 0.017\pm 0.0005$. Using the plausible relationships $\Gamma = 4\pi\delta n/\lambda$ and $\tau = \epsilon_0\epsilon/\sigma_{\mathrm{ph}}$ with $\epsilon = 30$, quite reasonable values $\delta n = (9\pm 0.1)\times 10^{-5}$ and $\sigma_{\mathrm{ph}} = 2\times 10^{-14}\ \Omega^{-1}\,\mathrm{cm}^{-1}$ are obtained for the effective refractive index change and the photoconductivity, respectively. Only the parameter m_0 with nearly 2% largely seems to overestimate the initial ratio of scattered to pump intensity. Nevertheless, in view of the

 ©2000 The American Physical Society

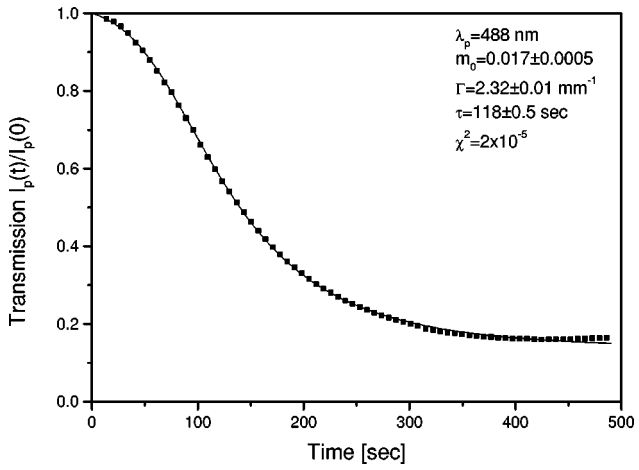

FIG. 1. Time dependence of the transmitted intensity during the writing process of parasitic gratings using extraordinarily polarized light of $\lambda_p = 488$ nm with an intensity of $I_p = 0.2\ \mathrm{W\,cm^{-2}}$. The solid line is a fit according to Eq. (1).

complicated dependence of light-induced scattering on material parameters and their dependence on spatial frequency $\boldsymbol{K}$, Eq. (1) fits the experimental data remarkably well. In the following we will consider only the steady-state limit where the transmission does not change any more. Figure 2 is a photograph of the intensity pattern on a screen placed 50 cm behind the crystal. The most prominent feature is that practically the whole scattered intensity is distributed along the direction parallel to the c axis of the crystal (pointing up). This structure is well known and was originally named c axis scattering. For media with nonlocal response it can usually be described in the framework of a one-species model by taking into account the tensorial nature of the electro-optic, dielectric, elasto-optic, and piezoelectric properties.[8] However, in $LiNbO_3$:Fe a puzzling point remains: The fact that the scattered intensity is amplified along both directions, the

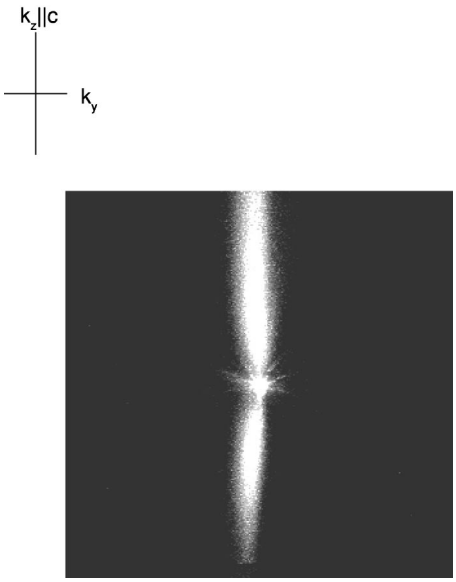

FIG. 2. Steady-state far-field intensity distribution of amplified scattered light induced by a pump beam ($\lambda_p = 488$ nm) propagating through a $LiNbO_3$:Fe sample along a direction perpendicular to the c axis (pointing upwards).

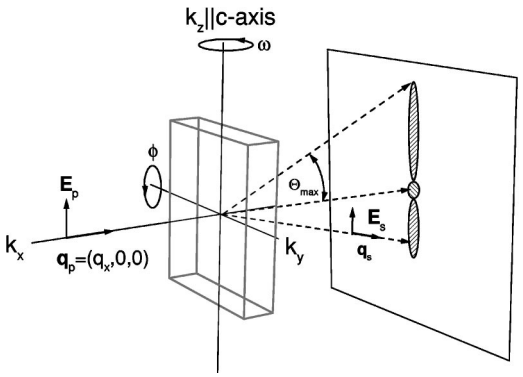

FIG. 3. Sketch of the experimental setup and geometry for transmission measurements during recording and reconstruction.

$+c$ *and* $-c$ direction. Possible models to explain this phenomenon are given in Refs 9 and 10.

We focus on a different point: the angular and spectral dependence of the transmitted intensity when reconstructing the parasitic hologram at low intensity (reading). Such investigations have previously been performed on standard holographic photoplates[6,7] or silver halides.[11] However, those substances are isotropic and need a chemical fixing procedure during which the structure shrinks. This complicates an analysis of the results. As such difficulties do not occur in photorefractive crystals, we obtain more direct and defined information about the phenomenon.

The general experimental setup and the geometry are sketched in Fig. 3. The mutually orthogonal rotation axes (ω, ϕ), the wave vectors of the incident $[\boldsymbol{q}_p = (q_x,0,0)]$ and the scattered $(\boldsymbol{q}_s)$ beams, as well as the far-field scattering pattern are presented schematically.

As a starting point we performed measurements of the transmitted intensity as a function of the RA. The rotation axis thereby was parallel to the crystallographic c axis of the crystal, the wavelength and the polarization of the beam were kept unchanged with respect to recording, whereas the intensity was decreased to 10^{-6} W cm^{-2} in order to keep changes of the parasitic refractive index structures during the investigations negligible. Rotation angles with respect to that geometry we denote by ω; a superscript m denotes the pertinent angles of incidence within the crystal (see Fig. 3).

In Fig. 4 the circles (top scale) show the transmittance for a writing and reading wavelength $\lambda_p = \lambda_r = 488$ nm. Another measurement using $\lambda_p = \lambda_r = 514$ nm led to a very similar curve not shown here. The transmission curve is symmetric with respect to the origin with a full width at half maximum (FWHM) of $\Delta\omega^m = 23$ mrad. We expect that this value depends on the thickness of the gratings, and hence on the geometrical thickness of the crystal. Note that the minimum of the transmission appears at zero RA.

In a second step we performed a rotation around an axis perpendicular to the c axis which we call ϕ rotation. All other conditions are kept unchanged compared to the previous measurement. The main difference is evident from Fig. 4 (crosses, bottom scale): The FWHM is nearly an order of magnitude smaller. The transmittance is shown as a function of the RA ϕ^m with $\omega = 0$. The curve is again symmetric; the FWHM is $\Delta\phi^m = 3.2$ mrad. The slightly different transmittance values at zero RA for ω and ϕ rotation, respectively,

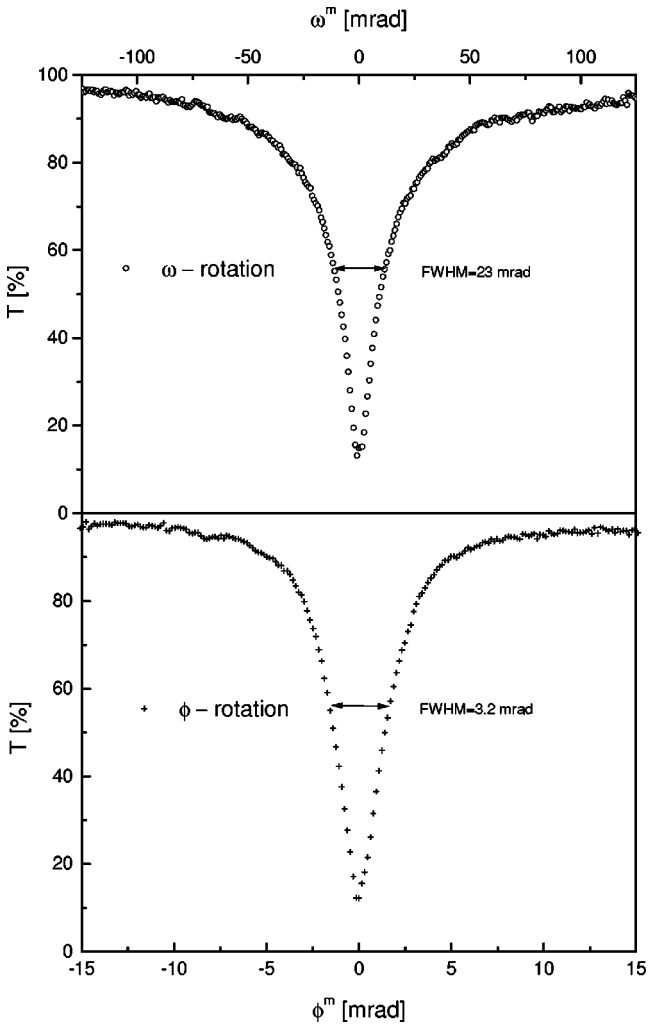

FIG. 4. Transmitted intensity as a function of the RA for $\lambda_p = \lambda_r = 488$ nm: for a rotation axis parallel to the optical axis (ω, open circles, top scale) or for a rotation axis perpendicular to the optical axis (ϕ, crosses, bottom scale).

result from the fact that for technical reasons we had to erase the gratings and to record them again prior to changing the rotation axis. Thereby we did not hit the identical spot of the sample.

We summarize at this point that if writing and reading wavelength coincide, the transmission curves are symmetric with respect to a rotation either parallel or perpendicular to the c axis but differ tremendously in half-width.

Next we determine the angular dependence of the transmission for a reading wavelength differing from the writing one. This is interesting as frequently reading and recording wavelength are not the same in standard holography techniques. The recording wavelength of the parasitic gratings was chosen to be either $\lambda_p = 514$ nm or $\lambda_p = 488$ nm. We then performed measurements of the angular dependence (rotation around c axis) of the transmittance for six different reading wavelengths of $\lambda_r = 514$, 501, 496, 488, 476, and 458 nm.

Let us first consider the case where $\lambda_r \leqslant \lambda_p = 514$ nm. The results of the measurements are shown in Fig. 5(a). The transmission curves have two minima at RA's which differ from zero RA (origin). The curves remain symmetric with

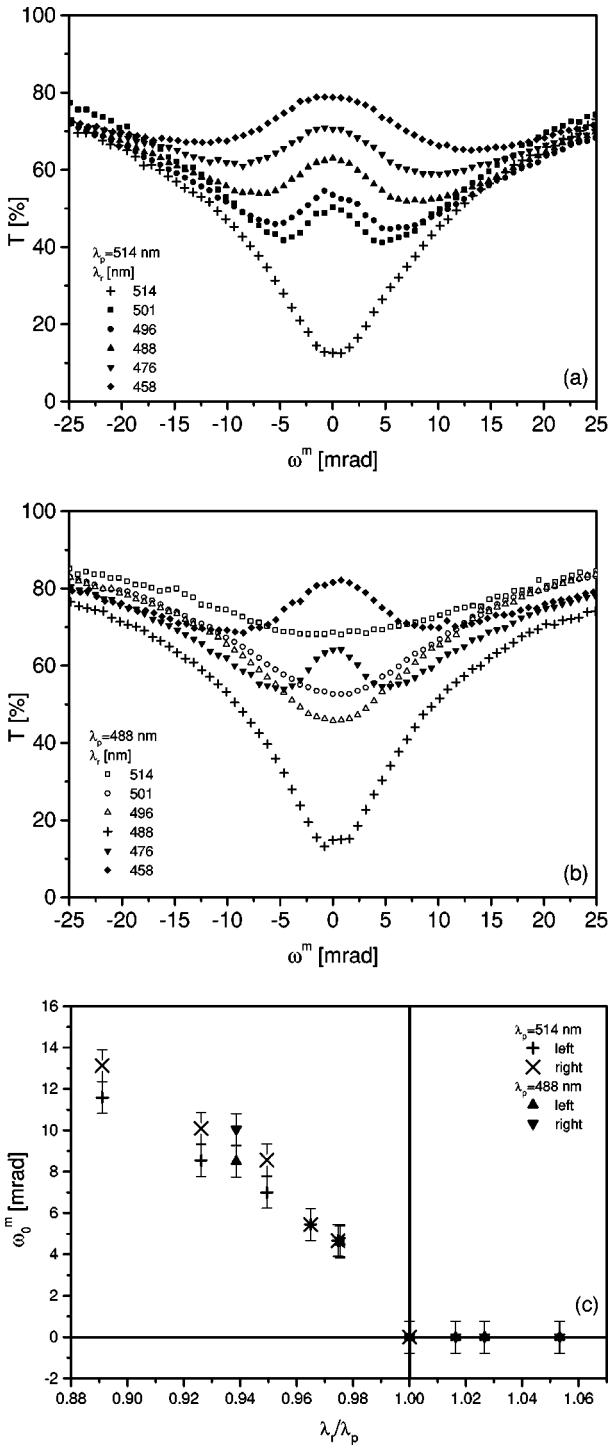

FIG. 5. Transmitted intensity as a function of the RA ω for different reading wavelengths (cf. text). (a) Recording wavelength $\lambda_p = 514$ nm; $\lambda_r \leqslant \lambda_p$. (b) Recording wavelength $\lambda_p = 488$ nm; $\lambda_r \geqslant \lambda_p$ or $\lambda_r < \lambda_p$. (c) RA ω_0^m of the minimum transmitted intensity for $\lambda_p = 488$ nm (solid triangles) and $\lambda_p = 514$ nm (crosses).

respect to the origin and reveal a maximum there. The RA ω_0 at which the minima occur increases as the wavelength deviates from the writing wavelength.

Finally we employed the situation where the wavelength of the reconstructing light wave is either higher, equal, or lower than the writing wavelength $\lambda_p = 488$ nm. Performing such an experiment leads to the transmission curves which are shown in Fig. 5(b). The curves which have been recon-

structed with $\lambda_r < \lambda_p$ resemble clearly the behavior of the previous case: two minima at RA's $\omega_0 \neq 0$. However, for $\lambda_r \geqslant \lambda_p$ only one minimum shows up at $\omega_0 = 0$, and the transmission value increases rather fast as the wavelength increases. In Fig. 5(c), the measured RA's ω_0 of the minimum transmittance for various reading wavelengths and the two writing wavelengths are plotted. The values of $+\omega_0$ and $-\omega_0$ which are presented do not differ within the limit of the error.

III. MODEL

The aim of this section is to outline a simple phenomenological (geometrical) model—based on the Ewald construction as developed in Refs. 6 and 7—which is able to explain the main features of the experimental observations and to use it for further predictions concerning the optimum reconstruction technique of standard holograms.

For simplicity let us assume that the pump beam is a plane wave $\boldsymbol{E}_p(\boldsymbol{q}_p)\exp(i\boldsymbol{q}_p \cdot \boldsymbol{x}) = (0,0,E_p)\exp(iq_x x)$ with amplitude E_p and wave vector $\boldsymbol{q}_p$. For elastic scattering without change of the polarization mode (so-called isotropic scattering) the scattered field generated by the pump wave may be described by $\int_{|\boldsymbol{q}_s|=\Omega/c} d^2 q_s \boldsymbol{E}_s(\boldsymbol{q}_s)\exp(i\boldsymbol{q}_s \cdot \boldsymbol{x})$, where Ω is the angular velocity. On the one hand, it seems hopeless to model holographic scattering because the scattered wave field has a complicated, *ab initio* unknown structure. On the other hand, an analysis is facilitated by the fact that we are in the limit of small modulation, i.e., $|m(\boldsymbol{K})| \ll 1$ holds for the complex function of the modulation $m(\boldsymbol{K}) = \boldsymbol{E}_p^*(\boldsymbol{q}_p) \cdot \boldsymbol{E}_s(\boldsymbol{q}_s)/I_0$ which characterizes the interference of the pump beam with the scattered wave field. Here I_0 denotes the total intensity. In this limit of small modulation the field $\delta n(\boldsymbol{x})$ of the refractive index changes resulting from the photorefractive effect in media with Pockels effect is predominantly the linear response of the interference pattern of the pump beam and the scattered wave field, i.e., for the Fourier transforms of the refractive index change and the linear-response function R of the photorefractive effect, the relationship $\delta n(\boldsymbol{Q}) = R(\boldsymbol{Q})m(\boldsymbol{Q})$ holds. As a consequence, $\delta n(\boldsymbol{Q})$ can differ from zero only for $\boldsymbol{Q} = \boldsymbol{K} = \boldsymbol{q}_s - \boldsymbol{q}_p$. In isotropic media nonzero values can therefore only be expected on spheres with radius $|\boldsymbol{q}_p| = q_x = \Omega/c = 2\pi n/\lambda_p$ and centers at $\boldsymbol{Q}_0 = (\pm q_x,0,0)$. The second sphere with its origin at $(+q_x,0,0)$ represents the complex-conjugate contributions for which $\delta n^*(\boldsymbol{Q}) = \delta n(-\boldsymbol{Q})$ holds since $\delta n(\boldsymbol{x})$ is a real function. It results from $m^*(\boldsymbol{K}) = \boldsymbol{E}_p(\boldsymbol{q}_p) \cdot \boldsymbol{E}_s^*(\boldsymbol{q}_s)/I_0$. As the first sphere is related to the reconstruction of the hologram and the second one to the generation of the optical phase conjugate, they are sometimes called the spheres of the primary and the conjugate images. In uniaxial crystals like $LiNbO_3$:Fe, the surface with nonzero $\delta n(\boldsymbol{Q})$ forms two ellipsoids. For the following discussion we disregard this detail as it is not relevant for the main features we want to discuss. However, we account for it in our calculations.

The necessary condition for the holographic scattering process to take place is that $R(\boldsymbol{Q}) \neq 0$. This being fulfilled with the amplitude $\boldsymbol{E}_s(\boldsymbol{q}_s)$, the modulation $m(\boldsymbol{Q})$ and hence $\delta n(\boldsymbol{Q})$ may increase with time, too. The region of the reciprocal space with optimum conditions for holographic amplification can then simply be read off from the stationary intensity distribution at the end of the process, which is the k_x-k_z plane in our case according to Fig. 2. The loci with largest $\delta n(\boldsymbol{Q})$ are the intersection of this plane with the two spheres discussed above, i.e., they form two circles lying in the k_x-k_z plane with centers at $\boldsymbol{Q}_0 = (\pm q_x,0,0)$, which will be called the ''writing circles'' in what follows.

Let us assume that a monochromatic plane wave with low intensity enters our crystal in which those parasitic holograms have been recorded. The intensity of the light scattered at each refractive index grating contains the information on the previously generated structure and is proportional to the square of the Fourier transform of the grating. This structure factor of the parasitic volume holograms is calculated for a crystal of thickness d and a uniform refractive index change $\delta n(x) = \delta n = \text{const}$ along the propagation direction as

$$I(k) \propto [\mathcal{F}\{\delta n\}(k)]^2 = \left(\delta n \frac{\sin(kd/2)}{kd/2} \right)^2 . \tag{2}$$

As we have to deal with a host of gratings with different $\boldsymbol{K}$ vectors, which are represented by the writing circles, we assume that the structure factor is equally distributed along those circles. We are aware that this is a simplification, as we know that refractive index gratings cannot be generated in certain directions for symmetry reasons. Nevertheless, we expect that the overall behavior will be revealed. Additionally, from the experimental observation (Fig. 2) we estimate that the largest contributing $\boldsymbol{K}_{\max}$ vector corresponds to a scattering angle of $\Theta_{\max}^m \approx 30°$ [cf. Fig. 3, Fig. 6(a)]. Moreover, we account for intensities rather than for amplitudes and phases. A consequence of the finite thickness of the gratings is that the width of the structure factor is finite, proportional to $1/d$, and resembles a ''cake'' [cf. Fig. 6(c)]. This region represents the part of the reciprocal space from which intensity can be supplied to a scattering process. Note that the writing circles in fact are smeared out and are rather a weighted circular ring.

Now we apply the Ewald construction to our problem: In reciprocal space the energy and momentum conservation for the scattering process is geometrically described by a sphere of radius $Q_r = 2\pi n/\lambda_r$ with its center in a point $\boldsymbol{Q}_0$ (''reading sphere''). The origin of the reciprocal space is always an element of both geometrical objects, namely the writing circles and the reading sphere. The totally scattered intensity is given by the integral value of the regions which contain intensity (writing circles) *and* satisfy the Bragg condition (reading sphere). Therefore, we have to consider only the intersection of the reading sphere with the k_x-k_z plane, which we call the ''reading circle''. Therefrom it is immediately evident that we obtain a maximum intensity of the scattered light if one of the writing circles and the reading circle are identical. In fact, by varying the parameters ω, ϕ, and λ_r we probe the $\boldsymbol{k}$ dependence of the structure factor integrated over the contour of the reading circle and hence obtain information on the gratings. Considering a variation of the parameters $\lambda_p, \lambda_r, \omega, \phi$ in which we are interested, we end up with a scenario that is schematically presented in Figs. 6(a) and 6(b). In this picture the gray rings are the writing circles and its gray scale symbolizes the intensity distribution in the

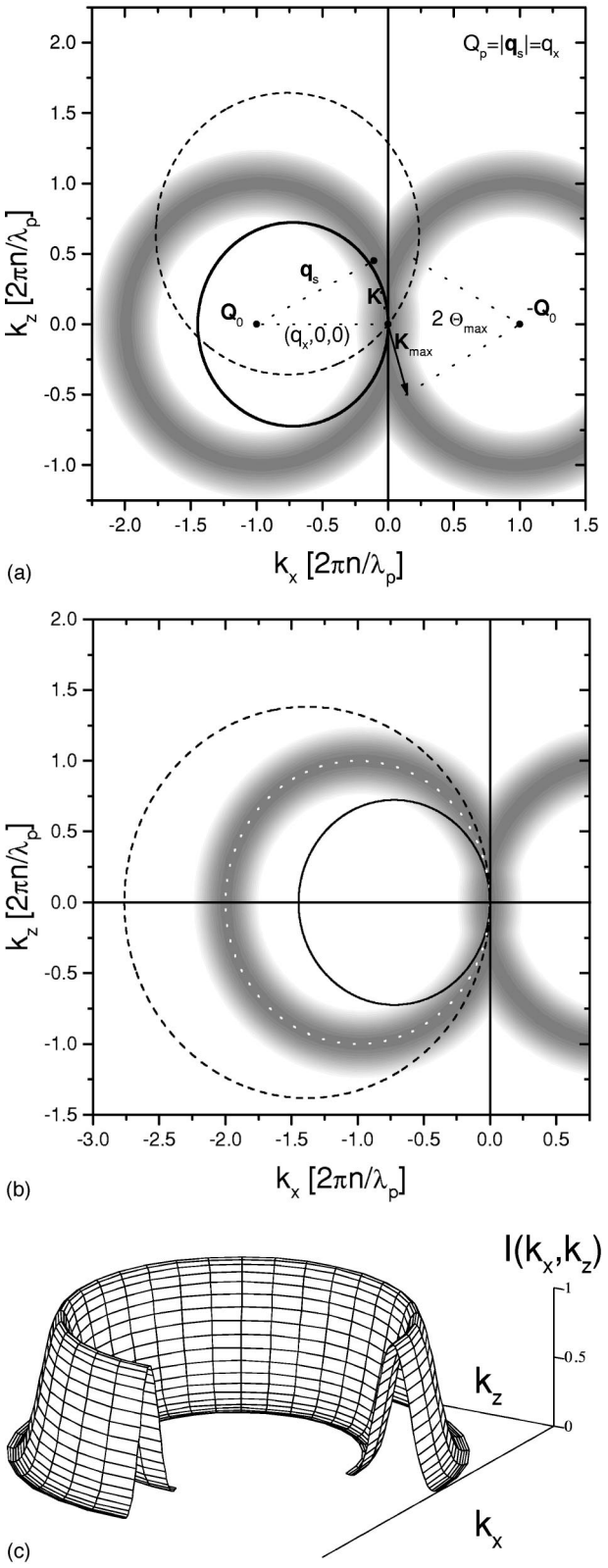

FIG. 6. Geometrical representation of the different scattering geometries performed in the experiments. The faint rings represent a projection of the structure factor (writing circles) onto the k_x-k_z plane. The ratio of the width to the radius is strongly exaggerated. The reading circles correspond to the following cases: (a) $\lambda_r=\lambda_p, \omega\neq 0, \phi=0$ (full line) and $\lambda_r=\lambda_p, \omega=0, \phi\neq 0$ (dashed line). (b) $\omega=0, \phi=0$: $\lambda_r>\lambda_p$ (full line); $\lambda_r=\lambda_p$ (dotted line); and $\lambda_r<\lambda_p$ (dashed line). (c) Structure factor distribution $\mathbf{I}(k_x,k_z)$.

k_x-k_z plane of the reciprocal space according to Eq. (2). Note that the width is strongly exaggerated for the sake of a better representation. The intersection of the Ewald sphere with that plane (the reading circle) is shown for the two different rotation axes: the bold solid line represents the reading circle for ω rotation, i.e., a rotation of the Ewald sphere out of the plane. The intersection results in a circle of smaller radius as compared to the reading circle at $\omega=0$; it shrinks. The dashed line, on the other hand, results from the intersection of the Ewald sphere with the k_x-k_z plane if we rotate the crystal perpendicular to the c axis (ϕ rotation). Unlike in the previous case, such an operation yields a circle of constant radius rotating around the origin $\boldsymbol{k}=\mathbf{0}$ of the reciprocal space. In Fig. 6(b) we show the case of $\omega=\phi=0$ for three different reading wavelengths: The dashed line represents a wavelength $\lambda_r<\lambda_p$ hence having a bigger radius of the reading circle in reciprocal space, whereas with the solid line $\lambda_r>\lambda_p$ it is vice versa. The white dotted line is related to the case $\lambda_r=\lambda_p$. Note that to some extent an ω rotation is equivalent to a change of the wavelength. Some particular cases will be discussed in the next section.

The scattered intensity I_S is proportional to the overlap of the structure factor (writing circles) and the Ewald sphere (reading circle). To obtain $I_S(\phi,\omega,\lambda_p,\lambda_r)$ we integrate the function of the structure factor of Eq. (2) along the reading circle:

$$I_S(\phi,\omega,\lambda_p,\lambda_r)=\int_{\mathcal{C}} I(k_x(\gamma),k_z(\gamma))\,d\gamma \tag{3}$$

with $\mathcal{C}$ a rectifiable path along the reading circle, where γ parametrizes that contour. Normalizing the total intensity to 1, the transmittance is given by $1-I_S$.

IV. DISCUSSION

Even without any calculation, we can already understand the main results of the experiments given in Sec. II qualitatively: The shape of the transmission curves for $\lambda_p=\lambda_r$, the difference of the FWHM for ω rotation and ϕ rotation, respectively, and the double-minimum structure for $\lambda_r<\lambda_p$. The model's predictions can be summarized as follows.

(i) For $\lambda_r=\lambda_p$ and a rotation around an axis parallel to the polar axis of the crystal (ω rotation): The radius of the reading circle shrinks according to $Q_r(\omega)=Q_r(\omega=0)\cos(\omega)$ (intersection of the Ewald sphere with the k_x-k_z plane) and its center moves towards the origin of the reciprocal space likewise [Fig. 6(a), solid line].

(ii) For $\lambda_r=\lambda_p$ and a rotation around an axis perpendicular to the polar axis of the crystal (ϕ rotation): The radius of the reading circle remains constant but its center moves on an auxiliary circle with radius Q_r around the origin $\mathbf{0}$ of the reciprocal space [Fig. 6(a), dashed line].

(iii) For $\lambda_r<\lambda_p, \phi=0, \omega\neq 0$: The reading circle is larger than the writing circle, so that an additional ω rotation will lead to a shrinkage of the reading circle. Therefore, at a certain angle $\pm\omega_0\neq 0$ the reading and writing circles will perfectly coincide, i.e., we obtain maximum diffraction for that angle leading to a double minimum structure in the transmission curves [cf. Fig. 5(a) and Fig. 8].

(iv) For $\lambda_r>\lambda_p, \phi=0, \omega\neq 0$: The reading circle is smaller than the writing circle. Therefore, the maximum diffraction

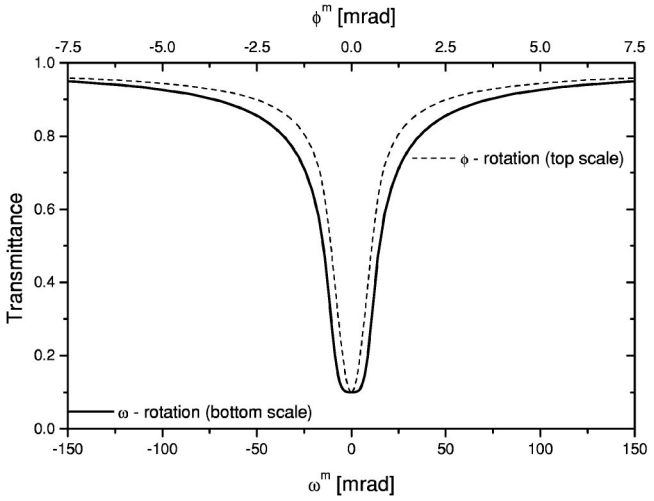

FIG. 7. Calculated transmittance as a function of the RA for different rotation axes: ω^m rotation (solid line) and ϕ^m rotation (dashed line) with $\lambda_p = \lambda_r = 488$ nm, $d = 2.55$ mm.

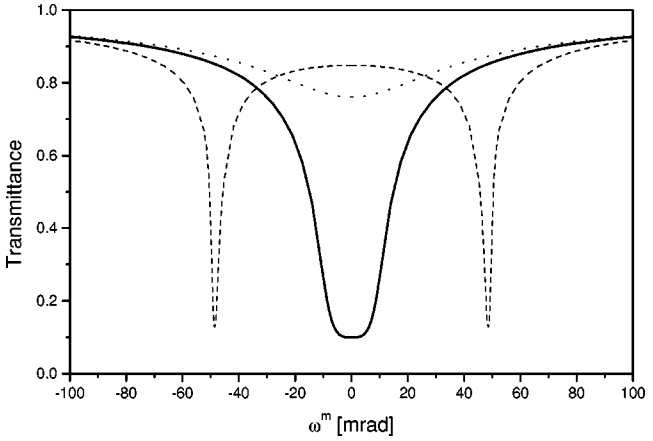

FIG. 8. Calculated transmittance as a function of the RA for ω rotation, $\lambda_p = 488$ nm: $\lambda_r = 487.5$ nm$< \lambda_p$ (dashed line); $\lambda_r = \lambda_p$ (solid line); and $\lambda_r = 488.2$ nm$> \lambda_p$ (dotted line) for $d = 2.55$ mm.

will occur at $\omega = 0$ but will be much less than in the case $\lambda_r = \lambda_p$ [cf. Fig. 5(b) and Fig. 8].

In Fig. 7 and Fig. 8 the calculated transmission curves for the various cases discussed above are shown. Figure 7 demonstrates that the FWHM of the transmission curves depends strongly on the rotation axes. This can be understood by having a look at Fig. 6(a): A rotation parallel to the c axis (ω, solid line in Fig. 7) diminishes the overlap of the writing and reading circles much less than a ϕ rotation (dashed line in Fig. 7) for the same angle. Hence the angular dependence of the resulting transmission curve of the latter is much more sensitive to deviations from the writing geometry. In Fig. 8 the ω dependence of the transmittance is shown for all possible relations between reading and writing wavelength. As already stated above, the shrinkage of the reading circle leads to a double minimum structure. The value ω_0 of this minimum transmission can be calculated easily to be

$$\omega_0^m = \arccos\left(\frac{Q_p}{Q_r}\right). \tag{4}$$

From Eq. (4) two aspects are interesting: The value ω_0 of the minimum depends only on the ratio of the writing and reading wavelength (and the dispersion of the refractive index), and for $\lambda_r > \lambda_p$ the right-hand side of the equation becomes an imaginary number. That is what we observe in the measurements: The minimum appears at $\omega_0 = 0$ in this case. Comparing the experimental data [Fig. 5(c)] to the predictions of the model, we have to admit that only a qualitative agreement is found. A quantitative comparison between the experiment and the model cannot be established. The evaluation of the minima for the different available writing wavelengths shows that the calculation leads to a much faster movement of the minima than observed in the experiments. Moreover, the depth of the minima should remain constant according to the model as we reach full matching of the reading and writing sphere in any case. The reason for the quantitative disagreement is quite obvious: For the model we assumed that the intensity of the scattered light does not extend to the k_y direction, which is a simplistic view of the experimental result shown in Fig. 2. Therefore, the model describes a limiting case where the scattering wave vectors $\boldsymbol{q}_s$ are restricted to a plane (two-dimensional) in contrast to the standard case (three-dimensional) as, e.g., realized experimentally in strontium barium niobate.[1] In the latter, one would expect the same angular dependence of the transmission for any rotation axis and the identical behavior for λ_p/λ_r and λ_r/λ_p, respectively. $LiNbO_3$:Fe reflects the main features of the two-dimensional case, but to describe its behavior quantitatively it is necessary to account for the contribution of the wave vectors pointing out of the k_x-k_z plane. Another feature particular to $LiNbO_3$:Fe which can be seen from Fig. 2 concerns the scattering pattern with respect to the $+c$ and $-c$ direction. From the viewpoint of symmetry, an amplification of scattered intensity is allowed only along one of those directions. The experiment refutes that argument but a fully symmetric pattern does not appear either. We did not account for such an asymmetry in our model as there is no need when describing the data presented in this work. Measuring the transmittance using $\lambda_p \neq \lambda_r$ and performing a ϕ rotation should reveal that asymmetry. Investigations on that problem as well as on the polarization dependence of the holographic scattering process are in progress.

In conclusion, we have measured the angular and spectral dependence of the transmitted intensity in $LiNbO_3$:Fe in the presence of parasitic gratings. The FWHM of the transmission is an order of magnitude lower when rotating around an axis perpendicular to the polar axis than it is when rotating around an axis parallel to it. By reconstructing the holograms with reading wavelengths higher than the writing wavelength, holographic scattering can be suppressed substantially. Otherwise a double minimum structure in the transmission curve appears. A model based on the Ewald construction qualitatively explains the obtained results.

ACKNOWLEDGMENTS

This work has been partially supported by the ÖAD-project A-2/1998. One of the authors (M.E.) is grateful for a grant from the Austrian Academic Exchange Service (ÖAD). It is a pleasure to acknowledge helpful discussions with Theo Woike. We thank Eckhard Krätzig for supplying the sample.

[1] R.A. Rupp, J. Seglins, and U. van Olfen, Phys. Status Solidi B **168**, 445 (1991).
[2] R.A. Rupp and F.W. Drees, Appl. Phys. B: Photophys. Laser Chem. **39**, 223 (1986).
[3] A. Fimia, A. Belendez, and L. Carretero, Proc. SPIE **2688**, 135 (1996).
[4] A. Belendez, I. Pascual, and A. Fimia, Opt. Quantum Electron. **25**, 139 (1993).
[5] M. Imlau, T. Woike, B. Schieder, and R.A. Rupp, Phys. Rev. Lett. **82**, 2860 (1999).
[6] M. Forshaw, Opt. Commun. **8**, 201 (1973).
[7] G. Riddy and L. Solymar, Electron. Lett. **22**, 872 (1986).
[8] G. Montemezzani *et al.*, Phys. Rev. A **52**, 1791 (1995).
[9] B.I. Sturman, Zh. Éksp. Teor. Fiz. **100**, 1071 (1991) [Sov. Phys. JETP **73**, 593 (1991)].
[10] V.V. Obukhovskii and A.V. Stoyanov, Fiz. Tverd. Tela (Leningrad) **29**, 2919 (1987) [Sov. Phys. Solid State **29**, 1678 (1987)].
[11] R.R.A. Syms and L. Solymar, Appl. Phys. B: Photophys. Laser Chem. **30**, 177 (1983).